Excitation spectrum for an inhomogeneously dipole-field-coupled superconducting qubit chain

Hou Ian,[1,2] Yu-xi Liu,[1,3,4] and Franco Nori[1,5]

[1]*Advanced Science Institute, RIKEN, Wako-shi, Saitama 351-0198, Japan*

[2]*Faculty of Science and Technology, University of Macau, Macau*

[3]*Institute of Microelectronics, Tsinghua University, Beijing 100084, China*

[4]*Tsinghua National Laboratory for Information Science and Technology (TNList), Tsinghua University, Beijing 100084, China*

[5]*Physics Department, The University of Michigan, Ann Arbor, Michigan 48109, USA*

(Received 27 January 2011; published 24 May 2012)

When a chain of N superconducting qubits couples to a coplanar resonator, each of the qubits experiences a different dipole-field coupling strength due to the wave form of the cavity field. We find that this inhomogeneous coupling leads to a dependence of the collective ladder operators of the qubit chain on the qubit-interspacing l. Varying the spacing l changes the transition amplitudes between the angular momentum levels. We derive an exact diagonalization of the general N-qubit Hamiltonian and, through the $N = 4$ case, demonstrate how the l-dependent operators lead to a denser one-excitation spectrum and a probability redistribution of the eigenstates. Moreover, we show that the variation of l between its two limiting values coincides with the crossover between Frenkel- and Wannier-type excitons in the superconducting qubit chain.

DOI: 10.1103/PhysRevA.85.053833 PACS number(s): 42.50.Pq, 42.50.Ct, 85.25.−j

I. INTRODUCTION

Superconducting quantum circuits have attracted considerable attention because of their capabilities (i) to demonstrate macroscopically the basic interaction of one "atom" and one photon in a cavity (e.g., [1,2]), (ii) to serve as a platform for testing many quantum optical phenomena (e.g., [3–7]), as well as (iii) to show its potential as a basis for quantum information processing (e.g., [8–11]).

While research on single-qubit interactions is more common, many recent articles also studied multiqubit interactions. Superconducting circuits with such interactions are also known as quantum metamaterials [12]. To be precise, the circuit system we consider here consists of a chain of N superconducting two-level qubits coupled to a photon mode in a superconducting coplanar waveguide resonator. Compared to the single-qubit version, it can manifest even more quantum phenomena, including plasma waves [13], controllable collective dressed states [14], and quantum phase transitions [15–18]. It also promises potential for various applications, including quantum simulators [19] and quantum memories [20].

Theoretical studies of multiqubit interactions with a photon often employ the Dicke model [21], where the Pauli operators are summed and transformed into a bosonic operator. In this approach, the chain of qubits is treated collectively as an atomic ensemble and the excited qubits are collectively regarded as one exciton mode. This theoretical simplification proves adequate when (i) the number of excitations in the system is low (e.g., in the so-called "one-photon" processes) and (ii) the number of qubits is large enough such that the interspacing L_q between neighboring qubits can be ignored compared to the photon wavelength L_p in the resonator (i.e., the qubits can be regarded as a continuum).

However, the question of how excitations arise in superconducting metamaterials when these two conditions are *not* met remains unanswered. In a realistic setting for a superconducting circuit, the number N of qubits present can range from one to, say, 10, but N would not be as large as the number of atoms we usually have for an alkaline atomic ensemble in an optical microcavity, which is typically greater than 10^5. Therefore, the Dicke model, which treats $N \to \infty$, does *not* apply well to the case of multiqubit superconducting circuits with $N \leqslant 10$.

When a chain of superconducting circuit qubits is arranged as a one-dimensional array [i.e., a superconducting qubit chain (SQC)], each qubit is *inhomogeneously coupled* to the circuit photon mode. In other words, each qubit has a *different* coupling strength to the photon field. This occurs naturally since, unlike its optical cavity quantum electrodynamics (QED) counterpart, the photon wavelength L_p is comparable to the qubit interspacing L_q in a superconducting circuit. The coupling strength thus depends on the position of the qubit relative to the photon wave form. The effect of the varying coupling strength becomes even more obvious if multimode couplings are taken into consideration. For example, the qubits on the antinodes of the wave form will couple most strongly, whereas those on the nodes will not couple.

The first step to understand and characterize this inhomogeneously coupled system (the aim of this article) is to obtain the energy spectrum of the collective excitation mode in the chain of qubits and to compare it with that of the Dicke model. We find that the inhomogeneity of the couplings incurs an algebraic deformation of the Pauli operators of the qubits [22–25]. We quantify this deformation through a "deformation factor," which is a function of the relative spacing $l = 2L_q/L_p$, and characterize the amount the inhomogeneous system deviates from the homogeneous case. The deformation factor modifies the spin operators of the collective qubit chain. Consequently, the excitation spectrum will not only be a function of the eigenenergy of the photon mode and the qubit level spacing, but is also highly related to the deformation factor and hence the relative spacing l.

Note that when atoms are confined to a cavity, the magnetic or laser field that is exerted on them is *uniform*. The strength of the interaction can be uniformly increased or decreased according to the density of the atoms. This macroscopic viewpoint does not differentiate between the identities of the

atoms. However, for circuit QED, the identities of the qubits are partially differentiated since the qubits can be categorized according to the values of their coupling strength to the photon mode. This partial differentiation has made understanding the inhomogeneous system a many-body physics question.

Our deformation algebraic approach here is a statistical approximation method that can be regarded as finding the average contribution of the coupling strength given by the SQC as a whole. In the end, the characterization (the excitation spectrum) of the SQC as an inhomogeneous system is not parametrized by the individual qubits, but by the relative spacing l. In other words, the spacing l is one extra degree of freedom peculiar to the inhomogeneous SQC, not seen in a homogeneous optical cavity.

We will first introduce the model and derive the deformation factor in Sec. II. With the deformation factor, new operation rules for the spin angular momentum operators are found by solving a difference equation in Sec. III. The general energy spectrum for n-qubit SQC is given in Sec. IV. We also derive in Sec. IV a one-excitation spectrum for a four-qubit SQC as a nontrivial case to show the effects of the inhomogeneity. Namely, the energy splittings between the eigenstates of the deformed coupling case shrink, while the probability amplitudes of the eigenstates are redistributed such that higher-photon occupations are favored.

In the final Sec. V, we will consider how the collective excitations on the SQC would emulate the excitons in atomic lattices, especially on how the varying spacing l can affect the distinct localizations of the SQC excitons to approach two limits, emulating the Frenkel and the Wannier exciton, respectively. Since the cavity photon is a standing wave instead of a propogating electromagnetic wave in a dielectric solid, we discuss the localization problem in the Fourier transform domain and observe from it how the emulated exciton can cross over from the Frenkel type to the Wannier type. We find that this crossover depends on a $(2N-1)$-th order trigonometric equation, whose solution corresponds to the asymptotic turning point from the deformed (inhomogeneously coupled) SQC to the undeformed (homogeneously-coupled) SQC.

II. INHOMOGENEOUS COUPLING MODEL

A. Inhomogeneous coupling

For a finite number N of spins in the SQC, the problem discussed here is similar to the Tavis-Cummings (TC) model [26,27], where all the spins are grouped into a total "large" spin. However, the exactly solvable TC model applies only when the coupling is homogeneous and when the eigenfrequencies between the qubits and the photon mode are equal. When the coupling is inhomogeneous, the large spin does not obey the usual commutation relations of the Pauli matrices, which the TC model assumes.

The new commutation relations of the large spin introduced by the inhomogeneity are pertinent to the deformed SU(2) Lie algebras. From these algebraic structures, we can establish a deformed dipole-field coupling model, of which the TC model is a special case. In the following discussion, we consider the typical case where the interqubit spacing is uniform. The coupling strength of each qubit to the photon field can, therefore, be written as a cosine function of a phase factor which is determined by the position jl of the jth qubit, where j is the reduced coordinate and l is the relative spacing introduced above.

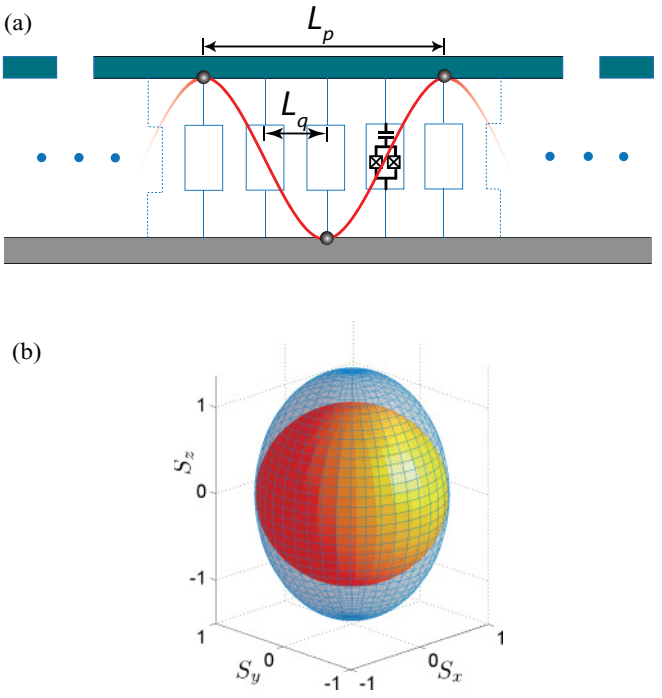

FIG. 1. (Color online) (a) Schematic diagram of a fraction of an SQC with spacing $l = 1$. The upper strip represents a coplanar resonator whose potential wave form of wavelength L_p is drawn as a sinusoidal curve, while the lower one represents a ground strip. The rectangles between the strips are qubits with interspacing L_q. The gray dots on the curve indicate the antinodes of the wave form. The blue dots indicate that only a fraction of the system is shown. (b) The elongation effect on the large spin due to inhomogeneous coupling. The ellipsoid shows a case of deformation $R_{N,l} = 0.5$. The unit sphere shows the spin under the usual homogeneous coupling.

The situation is illustrated in Fig. 1(a). A chain of qubits is sandwiched between the superconducting coplanar resonator and a superconducting ground strip. The photon mode providing different potential energies on the spins is shown by the red sinusoidal curve.

We use the operators $\{\sigma_{j,z}\}$ to denote Josephson junction qubits, and $\{a, a^\dagger\}$ to denote the operators for the single-photon mode. With the wave vector being the reciprocal of the photon field wavelength on the one-dimensional lattice, $k = 2\pi/L_p$, the dipole-field coupling is of the form $\sigma_{j,x}[a\cos(j\pi l) + \text{H.c.}]$. Under the rotating wave approximation, the Hamiltonian can be written as ($\hbar = c = 1$),

$$H = \omega_q \sum_{j=0}^{N-1} \sigma_{j,z} + \omega_0 a^\dagger a + \eta \sum_{j=0}^{N-1} \cos(j\pi l)[\sigma_{j,+} a + \sigma_{j,-} a^\dagger], \tag{1}$$

where ω_q is the eigenenergy of the spins, ω_0 the mode frequency of the photon, and η the coupling amplitude.

To diagonalize the Hamiltonian in Eq. (1), we introduce the "large spin" operators: the magnetic moment or z-direction

collective spin operator,

$$S_z = \sum_{j=0}^{N-1} \sigma_{j,z}, \tag{2}$$

which is no different from the homogeneous case, and the paired raising and lowering operators,

$$S_+ = \sum_{j=0}^{N-1} \sigma_{j,+} \cos(j\pi l), \tag{3}$$

$$S_- = \sum_{j=0}^{N-1} \sigma_{j,-} \cos(j\pi l), \tag{4}$$

which have the special sinusoidal dependence on l due to the inhomogeneity. The commutator of the paired ladder operators *no* longer equals to $2S_z$ but has an additional term due to the cosine coefficients (i.e., $[S_+,S_-] = 2\Sigma_z$) with

$$\Sigma_z = S_z + \sum_{j=0}^{N-1} \sin[j\pi(1+l)] \sin[j\pi(1-l)]\sigma_{j,z}. \tag{5}$$

The detailed derivation is shown in Appendix A 1. Note that in the usual circuit QED system [2], where only one spin is placed at midway, the spacing l equals to 2, for which the latter term in Σ_z vanishes. This is the limiting case which corresponds to the Wannier type of excitation, where the set of spin operators retains the usual structure of an undeformed SU(2) algebra.

B. Deformed algebraic structure

When the second term of Σ_z does not vanish, the algebraic structure is called deformed [22–25]. In order to quantify the deformation, the commutator of the ladder operators needs to be expressed as a function of S_z [i.e., $\Sigma_z = f(S_z)$]. To find this function f, we consider an underlying manifold, on which there is a local point, say the origin 0, where we define a tangent space with the Pauli z matrices $\{\sigma_{j,z}\}$ being its basis vectors, since these matrices are linearly independent. The operator S_z, defined above with uniform coefficients, can be deemed a vector in this tangent space; the operator Σ_z is then another vector dependent on the parameter l and is a deviation or deformation from S_z. Thus, the first-order approximation of Σ_z with respect to S_z is its projection onto the vector S_z. That is, since the cosine coefficients are bounded, we can use their Hilbert-Schmidt norm,

$$\langle \Sigma_z, S_z \rangle = \mathrm{tr}(\Sigma_z^* S_z) = N + \sum_{j=0}^{N-1} \cos(2j\pi l), \tag{6}$$

and the Schmidt decomposition [28] to write $\Sigma_z = R_{N,l} S_z$ as a deformation of the original z-spin operator where

$$R_{N,l} = \frac{1}{4N} \left\{ 2N + 1 + \frac{\sin[(2N-1)\pi l]}{\sin(\pi l)} \right\} \tag{7}$$

is the deformation factor (cf. Appendix A 2 for this derivation). The commutator of the ladder operators can now be expressed as

$$[S_+,S_-] = 2R_{N,l} S_z, \tag{8}$$

where $R_{N,l}$ has a limiting value of one when $l \to 0$ or $l \to \infty$, for which the usual structure used in the TC model is retained.

Since the deformation factor $R_{N,l}$ does not affect the commutation relations between the ladder operators and the z spin, the large-spin operators $\{S_z,S_+,S_-\}$ form a specific deformed algebra [22,23] and not the more general type [24]. The Casimir operator,

$$C = S_- S_+ + h(S_z), \tag{9}$$

of the algebra, which equals to the undeformed spin momentum square, $S^2 = S_x^2 + S_y^2 + S_z^2$, for the homogeneous coupling case, is accordingly deformed. Through solving a recursive relation (cf. Appendix A 3 for details), we find $h(S_z) = R_{N,l}(S_z^2 + S_z)$ and hence,

$$C = S_x^2 + S_y^2 + R_{N,l} S_z^2, \tag{10}$$

which shows that the spin momentum is *reduced* along the z direction:

$$S^2 = S_x^2 + S_y^2 + R_{N,l} S_z^2. \tag{11}$$

To visualize this reduction of the spin momentum, we can take a unit value for the spin moment and let the Casimir operator be represented by a unit sphere in three-dimensional space for the undeformed case. With $R_{N,l} \leqslant 1$, the deformation would be an elongation of the unit sphere, along the z axis, to an ellipsoid, while the x- and y-semi-minor axes remain unchanged, as shown in Fig. 1(b).

III. OPERATION RULES

If we consider the unit sphere of Fig. 1(b) as a Bloch sphere on which the large spin prescribes its N levels, its elongation due to deformation will accordingly modify the transitions between the levels. Since the spin-up and the spin-down momenta do not change, which are still $\omega_q N/2$ and $-\omega_q N/2$, the narrow part of the ellipsoid effectively squeezes the transition probabilities.

More precisely, we consider an arbitrary eigenstate $|r,m\rangle$, for which

$$S_z |r,m\rangle = m |r,m\rangle , \tag{12}$$

$$S^2 |r,m\rangle = r(r+1) |r,m\rangle . \tag{13}$$

The ladder operators result in an (r,m)-dependent off-diagonal matrix element $\alpha_m^{(r)}$, that is,

$$S_+ |r,m\rangle = \alpha_m^{(r)} |r,m+1\rangle , \tag{14}$$

$$S_- |r,m\rangle = \alpha_{m-1}^{(r)} |r,m-1\rangle . \tag{15}$$

By examining the diagonal elements of the commutator of the ladder operators, we find a difference equation $(\alpha_m^{(r)})^2 - (\alpha_{m-1}^{(r)})^2 = -2m R_{N,l}$. With the value $\alpha_{-r}^{(r)} = 0$, the equation can be solved to give the deformed off-diagonal matrix elements or transition probabilities for the ladder operators,

$$\alpha_m^{(r)} = \sqrt{R_{N,l}(r-m)(r+m+1)}. \tag{16}$$

See Appendix B for its derivation.

Geometrically speaking, the deformation process is a homeomorphism with a redefined metric $g = (1,1,R_{N,l})$. Since $R_{N,l} \leqslant 1$, the metric norm is less than unity. The

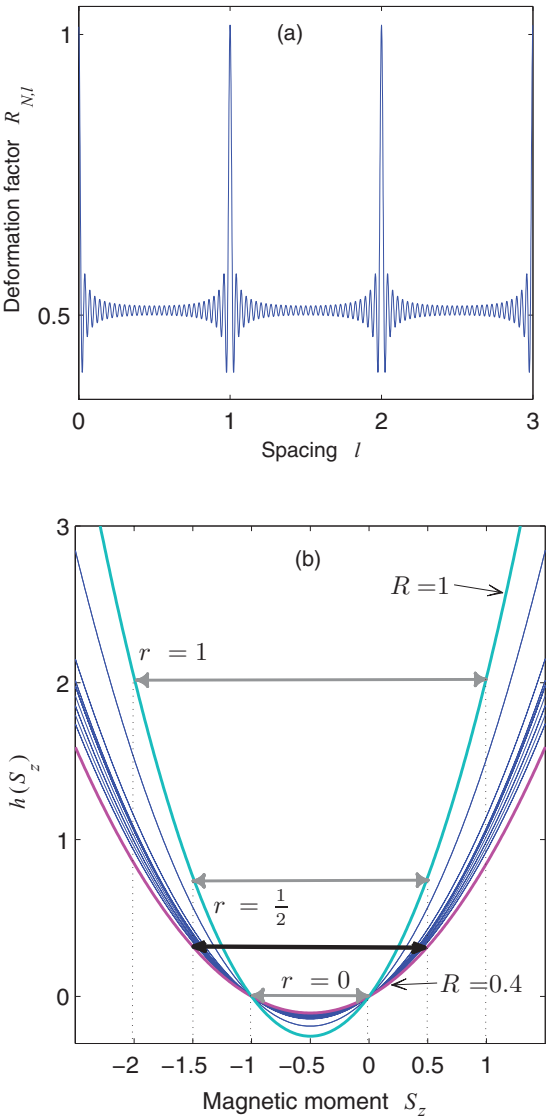

FIG. 2. (Color online) (a) The deformation factor $R_{N,l}|_{N=30}$, as an oscillating function of the qubit spacing l. (b) Plot of the function $h(S_z)$ for various values of $R_{N,l}$. The top and bottom boldened curves correspond to $R_{N,l}=1$ and 0.4, respectively. The gray-shaded double arrows indicate three spin levels of the underformed SQC, while the black arrows show the $r=1/2$ level of the deformed case.

deformation does not affect the level spacings of the magnetic moment S_z: The number m still takes $(2r+1)$ values (i.e., the ellipsoid is homeomorphic to the sphere). But the transition amplitudes to traverse the sphere decrease: If we start with a spin-up state $|r,r\rangle$ and finish with a spin-down state $|r,-r\rangle$, then all iterations with $S_-|r,m\rangle=\alpha^{(r)}_{m-1}|r,m-1\rangle$ have $\alpha^{(r)}_m$ smaller than the original $\bar{\alpha}^{(r)}_m=\sqrt{(r-m)(r+m+1)}$ (i.e., the ellipsoid is not isometric to the sphere).

The deformation factor expressed in Eq. (7) is an oscillating function of l, where the sine in the numerator determines the period of oscillation and the sine in the denominator determines the period of the envelope. Therefore, the spin angular momentum of the SQC would be *oscillating* between the unit sphere and the ellipsoid, depending on the qubit spacing l. The plot of $R_{N,l}$ in Fig. 2(a) for an SQC of $N=30$ qubits shows a typical case with envelop of period 1 and local minimum of 0.4. The function $h(S_z)$ associated with this deformation factor is a parabola of the magnetic moment S_z. For a nontrivial deformation $R_{N,l}<1$, this parabola flattens and the spin levels become denser. The curvature of the parabola decreases while its minimum value $-R_{N,l}/4$ increases. As shown in Fig. 2(b), the black (gray) arrow indicates the spin level $r=1/2$ for the deformed $R_{N,l}=0.4$ (undeformed $R_{N,l}=1$) case of SQC. So varying l makes the curve $h(S_z)$ oscillate between the boldened curves that correspond to $R_{N,l}=0.4$ and $R_{N,l}=1$, respectively. We can also observe that the level splittings are reduced, reflecting the elongated structure of the Bloch sphere in Fig. 1(b) and the modified operation rule of Eq. (16).

IV. DEFORMED SPECTRUM

Equipped with the modified operation rules, we can diagonalize the Hamiltonian in Eq. (1). First, we split the Hamiltonian into two parts:

$$H_0=\omega_0(S_z+a^\dagger a), \tag{17}$$

$$H_1=\tilde{\omega}_0 a^\dagger a+\eta(S_+a+S_-a^\dagger). \tag{18}$$

Let u be the number of total excitations and hence the eigenvalue of H_0. Let n be the number of photons in the system such that the SQC magnetic moment is $m=u-n$. Let v be the eigenvalue of the interaction part H_1, where $\tilde{\omega}_0=\omega_0-\omega_q$.

The eigenvector of the Hamiltonian can then be expanded as a superposition of different configurations of photon number and spin states:

$$|u,r\rangle=\sum_n c_n|n;r,u-n\rangle\,. \tag{19}$$

The expansion coefficients c_n satisfy a recursive relation [27]:

$$c_{n+1}\sqrt{n+1}\alpha^{(r)}_{u-(n+1)}-c_n\tilde{v}_n+c_{n-1}\sqrt{n}\alpha^{(r)}_{u-n}=0, \tag{20}$$

where $\tilde{v}_n=(v-\tilde{\omega}_0 n)/\eta$.

The solution reads

$$c_n=\sum_{p=0}^{\lfloor n/2\rfloor}(-1)^p(R_{N,l})^{p-n/2}\mathscr{C}_{n,p}. \tag{21}$$

$\mathscr{C}_{n,p}$ can be regarded as a probability amplitude contribution to the n-photon state from a set of corresponding qubit chain states indexed by p:

$$\mathscr{C}_{n,p}=\frac{P_n}{\sqrt{n!}}\sum_{\langle j_1\cdots j_k\cdots j_{\lfloor n/2\rfloor}\rangle}\cdots\sum\prod_{k=1}^{p}\frac{(j_k+1)}{\tilde{v}_{j_k}\tilde{v}_{j_k+1}}\left[\bar{\alpha}^{(r)}_{u-(j_k+1)}\right]^2, \tag{22}$$

where $P_n=\prod_{j=0}^{n-1}\tilde{v}_j/\bar{\alpha}^{(r)}_{u-(j+1)}$ and $\langle j_1\ldots j_k\ldots j_{\lfloor n/2\rfloor}\rangle$ represents an index set of descending order $\{\forall k<l:0\leqslant j_l\leqslant j_k-2;0\leqslant j_1\leqslant n-2\}$. We can see from Eq. (21) that the operation rules discussed in the preceding paragraphs have made the probability amplitudes deformation dependent, thus l dependent. This will consequently lead to a redistribution of probabilities for different photon states. See Appendix C 1 for the derivation of these coefficients $\mathscr{C}_{n,p}$.

The simplest nontrivial example of this deformation effect can be seen in Table I, where we consider the one-excitation

TABLE I. Configurations $|n;r,m\rangle$ and probability amplitudes c_n for the one-excitation spectrum of a SQC with $N = 4$ qubits and spacing $l = 2/3$. Each ○ indicates one photon while ↑ or ↓ denotes the spin state of each qubit. Here, $\tilde{v}_n = (v - \tilde{\omega}_0 n)/\eta$.

$u = 1$ $r = 2$	$\begin{cases} n = 0 \\ m = 1 \end{cases}$	$\begin{cases} n = 1 \\ m = 0 \end{cases}$	$\begin{cases} n = 2 \\ m = -1 \end{cases}$	$\begin{cases} n = 3 \\ m = -2 \end{cases}$
Photon	−	○	○○	○○○
Spin config.	↓↑↑↑ ↑↓↑↑ ↑↑↓↑ ↑↑↑↓	↑↑↓↓, ↓↓↑↑ ↑↓↓↑, ↓↑↑↓ ↑↓↑↓, ↓↑↓↑	↑↓↓↓ ↓↑↓↓ ↓↓↑↓ ↓↓↓↑	↓↓↓↓
c_n	1	$\frac{\tilde{v}_0}{\sqrt{6}R}$	$\frac{\tilde{v}_0\tilde{v}_1}{6\sqrt{2}R} - \frac{1}{\sqrt{2}}$	$\frac{\tilde{v}_0\tilde{v}_1\tilde{v}_2}{12\sqrt{6}R^{3/2}} - \frac{\tilde{v}_2+2\sqrt{6}\tilde{v}_0}{12\sqrt{R}}$

($u = 1$) spectrum of a four-qubit SQC with spacing $l = 2/3$. The deformation factor in this case is $R_{N,l} = 5/8$. For a weakly coupled SQC with $|\tilde{\omega}_0| \gg \eta$, the eigenenergies for the four levels are given by (cf. Appendix C2 for the derivation)

$$E_{\pm,\pm} = \omega_q + \tfrac{3}{2}\tilde{\omega}_0 \pm \tfrac{1}{2}\left[5\tilde{\omega}_0^2 \pm 4\tilde{\omega}_0\left(\tilde{\omega}_0^2 + 36R_{N,l}\eta^2\right)^{1/2}\right]^{1/2}. \tag{23}$$

For a deformation factor $R_{N,l} < 1$, the splittings between these dressed levels are suppressed. In addition, if we substitute the value of v into the coefficients c_n, we will find that c_1 is greater than that of the undeformed case, c_2 (c_3) increases by a greater proportion than c_1 (c_2), while c_0 remains equal to one. Therefore, the probability distribution shifts toward the end that favors states with a greater number of photons and less degeneracy.

V. EXCITONS IN THE QUBIT CHAIN

A. Background on excitons

When an atomic lattice is excited by some incident radiation, a number of atoms absorb the energy, creating simultaneously excited electrons from the valence band and corresponding excited holes from the conduction band (see Ref. [29] for a concise review). Multiply-excited electron-and-hole pairs arise at different lattice points in a crystal, forming an excitation wave. Frenkel showed that several superposed excitation waves compose a single excitation packet or exciton that can propagate in the lattice. However, if the electron-hole attraction energy is sufficiently large, the electrons are tightly bound to their ionic cores, unable to propagate in the lattice. In other words, the electron-hole pairs in their excited orbits are regarded as localized while the exciton (a.k.a., the Frenkel exciton) is not necessarily localized to any lattice point. As a result, Frenkel concluded that certain dielectric materials can conduct heat current, which are carried by the excitons while they cannot conduct electric currents, which are carried by the electrons.

Later, Wannier found that even the excited electron-hole pairs are not necessarily confined to their individual lattice cell. Due to different electronic configurations, insulators can have either localized or delocalized electron-hole pairs. He quantified this argument by showing that a definite portion of the total multiplicity of the electron states are gapped from the excited Bloch band. As a result, the electron-hole pairs of certain dielectric materials are indeed ionizable to the Bloch continuum and conduct electric current. In such a case, there is no need to differentiate between the excitation waves, the excitation packets, and the excitons. The electron-hole pairs are themselves the excitons, delocalized and propagating in the atomic lattice (a.k.a., the Wannier exciton).

Whether it is a Frenkel exciton or a Wannier exciton, the basic phenomenon is that of a collective quasiparticle excitation, which can be theoretically studied using the Dicke model; that is, the excitons obey bosonic statistics in the large-N limit, where N is the total number of atoms in the atomic lattice. By considering the excitons as bosonic operators, various aspects and properties of different materials have been studied. On one hand, the tightly bound Frenkel excitons are used to study, for example, the radiation and optical dynamics of a crystal slab of ionic compound [30]. On the other hand, the study of kinetics and scattering in semiconductors, especially the Bose-Einstein condensates in semiconducting materials, are modeled after the ionizable electron-hole pairs or Wannier excitons (see, e.g., [31] for a detailed review).

Therefore, there are two ways to categorize the collective excitations into Frenkel excitons and Wannier excitons. One way accords to the value of the binding energy between electrons and holes for different dielectrics: the Frenkel excitons typically possess higher binding energy than the Wannier excitons. The other way is geometric: by determining how the photon energy is absorbed. The base of Frenkel excitons are excitation waves, which designates an uneven absorption of energy across a group of neighboring atomic cells in the lattice. The base of Wannier excitons are excited electron-hole pairs, which stem from independent atomic cells after each individually absorbs some certain energy quanta. In fact, according to the latter interpretation, it has been shown [32] that the Frenkel excitons and the Wannier excitons coexist in alkali compounds. The two types of excitations are linear combinations of each other. Recent experiments have verified that the two types are convertible to each other in some hybrid semiconductors [33].

B. Emulated excitons and their crossover in SQC

To a large extent, a superconducting qubit macroscopically emulates the quantum mechanical behavior of a two-level atom. Their mathematical models are identical for weak electromagnetic couplings. Extending this concept to many superconducting qubits, the SQC collectively emulates a

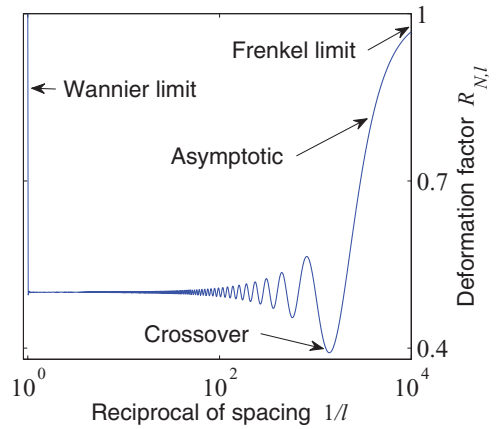

FIG. 3. (Color online) Semilog plot of the deformation factor $R_{N,l}$ versus $1/l$ over one period, showing the Wannier limit on the left end and the Frenkel limit on the right end of the horizontal axis. The number of qubits is set to $N = 1000$.

one-dimensional atomic lattice. Particularly, the excited qubits are functionally identical to the excited atoms in layered crystal slabs as described in Ref. [30]. Moreover, the excitations induced by the cavity photons in the superconducting stripline obey bosonic statistics in the large-N limit as we have shown in Sec. II, just like those of the regular excitons.

There remains the question of which type of excitons do the excitations in SQC emulate. If we adopt the geometric intepretation, both types of excitons coexist in the SQC lattice as in the alkali compounds and hybrid semiconductors. The emulated exciton type depends on whether the neighboring qubits are excited individually or excited unevenly as a wave. This dependence relies exactly on the relative spacing l of the SQC.

In the large l limit [i.e., when the interqubit spacing L_q is much larger than the photon wavelength L_p ($L_q \gg L_p$)] we assume that the excitation induced by the uniform dipole-field coupling produces emulated Wannier excitons evenly at each lattice site. In the small l limit [i.e., when $L_q \ll L_p$ (in particular, for the base mode in the strip line, a single-photon wavelength extending over all the qubits], an excitation wave is formed on the SQC; this type of excitation is considered as the emulated Frenkel excitons.

Note that when l tends to either zero or infinity in Eq. (5), Σ_z falls back to S_z and the regular SU(2) algebra for the commutators is obtained. Thus, it is justified that in the large-N limit, the low-energy excitation becomes bosonic for both Wannier and Frenkel excitons. To determine when the emulated exciton crosses from Wannier- to Frenkel-type, we plot in Fig. 3 the deformation factor versus the reciprocal of the spacing over $10^{-4} < l < 1$, where we can see the asymmetry between the left edge ($1/l \to 0$) for the Wannier limit and the right edge ($1/l \to \infty$) for the Frenkel limit. Setting $dR_{N,l}/dl = 0$, we obtain the trigonometric equation,

$$\tan[(2N-1)\pi l] = (2N-1)\tan(\pi l). \tag{24}$$

Transforming Eq. (24) to $U_{2N-1}(\cos \pi l) = 2N \times T_{2N-1}(\cos \pi l)$, where T_{2N-1} (U_{2N-1}) is the Chebyshev polynomial of the first (second) kind, we can observe that it is a $(2N-1)$th-order polynomial equation. Hence, the curve has $(2N-1)$ local extrema in exactly $(N-1)$ oscillations from the Wannier end to the asymptotic Frenkel end. Between these two limits, the excitation has various degrees of deformation and the crossover is continuous. We can regard the crossover point to be the absolute minimum before the deformation factor asymptotically approaches one. This point approaches 0 when $N \to \infty$. For the case illustrated in Fig. 3 with $N = 1000$, a numerical estimation gives the crossover at $l = 7.16 \times 10^{-4}$, or a length of 2800 spins per photon wavelength.

VI. CONCLUSION

We have studied the inhomogeneous coupling between a SQC and a superconducting coplanar resonator, which leads to a set of deformation-dependent operation rules of spin momentum. The modified rules correspond to tighter energy spacings and a shift of the probability distribution of spin levels. We also found that the excitations in the SQC emulated both the Frenkel and Wannier exciton, but at two limiting length of the qubit spacing l, between which a crossover can be determined through a polynomial equation with l as the variable. Since the usual excitons give rise to many cooperative radiation phenomena such as superradiance and superfluorescence, we predict that a similar effect will arise in the SQC when multiple photon modes are filled in the cavity. These radiation effects, specifically the transportation effect of the radiated photons from the SQC excitons can be studied with the applications of quantum information propagation in our future researches.

ACKNOWLEDGMENTS

H.I. acknowledges support from University of Macau Grant No. SRG003-FST12-IH. F.N. acknowledges partial support from LPS, NSA, ARO, DARPA, AFOSR, National Science Foundation Grant No. 0726909, JSPS-RFBR Contract No. 09-02-92114, MEXT Kakenhi on Quantum Cybernetics, and Funding Program for Innovative R&D on S&T. Y.X.L. acknowledges support from National Natural Science Foundation of China Grants No. 10975080 and No. 61025022.

APPENDIX A: DERIVATION OF THE DEFORMATION FACTOR

1. Commutation relation

The commutator of the ladder operators can be computed as follows:

$$\begin{aligned}[S_+, S_-] &= \sum_{j,k=0}^{N-1} \cos(j\pi l)\cos(k\pi l)[\sigma_{j,+}, \sigma_{k,-}] \\ &= 2\sum_{j=0}^{N-1} \cos^2(j\pi l)\sigma_{j,z} \\ &= S_z + \sum_{j=0}^{N-1} \cos(2j\pi l)\sigma_{j,z}.\end{aligned}$$

To use a consistent notation, we write the right-hand side as $2\Sigma_z$ and extract S_z from the second term,

$$\begin{aligned} 2\Sigma_z &= 2S_z + \sum_{j=0}^{N-1} [\cos(2j\pi l) - \cos(2j\pi)]\,\sigma_{j,z} \\ &= 2S_z + 2\sum_{j=0}^{N-1} \sin[j\pi(1+l)]\sin[j\pi(1-l)]\,\sigma_{j,z}, \end{aligned}$$

which gives Eq. (5).

We can also check that other commutation relations are preserved:

$$\begin{aligned} [S_z, S_\pm] &= \sum_{j,k=0}^{N-1} [\sigma_{k,z}, \sigma_{j,\pm}\cos(j\pi l)] \\ &= \sum_{j=0}^{N} \pm\sigma_{j,\pm}\cos(j\pi l) \\ &= \pm S_\pm, \end{aligned}$$

from which we conclude that the newly defined operators $\{S_z, S_+, S_-\}$ form a Polychronakos-Rocek type of deformed SU(2) algebra.

2. Deformation factor

First, we recognize that each qubit $\sigma_{j,z}$ has two orthonormal basis vectors $\{|e_j\rangle, |g_j\rangle\}$ for a fixed relative coordinate j and hence $\{|\epsilon_k\rangle : |\epsilon_k\rangle \in \{|e_j\rangle, |g_j\rangle, j = 0, \ldots, N-1\}\}$ forms an orthonormal basis for the Hilbert space $\mathcal{H}$ that spans all the qubits on the chain. Then S_z for the original spin angular momentum and Σ_z for that of the inhomogeneous SQC become operators on this Hilbert space $\mathcal{H}$. Since the sinusoidal functions $\cos(j\pi l)$ are bounded, we can define the Hilbert-Schmidt inner product as

$$\begin{aligned} \langle \Sigma_z, S_z\rangle = \mathrm{tr}(\Sigma_z^* S_z) &= \sum_{k}^{2N} \langle \epsilon_k | \Sigma_z \cdot S_z | \epsilon_k \rangle \\ &= \sum_{k}^{2N} \langle \epsilon_k | \sum_{j,l=0}^{N-1} \cos^2(j\pi l)\sigma_{j,z}\cdot\sigma_{l,z}\,|\epsilon_k\rangle \\ &= \sum_{k}^{2N} \langle \epsilon_k | \cos^2(\lfloor k/2\rfloor \pi l)\sigma_{\lfloor k/2\rfloor,z}\cdot\sigma_{\lfloor k/2\rfloor,z}\,|\epsilon_k\rangle \\ &= \sum_{k}^{2N} \cos^2(\lfloor k/2\rfloor \pi l) \\ &= \sum_{j}^{N} 2\cos^2(j\pi l), \end{aligned}$$

which equals to Eq. (6). We can then write the approximation of Σ_z as a Schmidt projection on S_z,

$$\begin{aligned} \Sigma_z &\approx \frac{\langle \Sigma_z, S_z\rangle}{\langle S_z, S_z\rangle} S_z \\ &= \frac{N + 1 + \sum_j \cos(2j\pi l)}{2(N+1)} S_z \\ &= \left[\frac{1}{2} + \frac{1}{2N}\sum_{j=0}^{N-1}\cos(2j\pi l)\right] S_z \\ &= R_{N,l} S_z, \end{aligned}$$

where $R_{N,l}$ denotes the deformation factor. Its expression can be further simplified to

$$\begin{aligned} R_{N,l} &= \frac{1}{4N}\left[2N + 1 - \cos(2N\pi l) + \frac{\sin(2\pi l)\sin(2N\pi l)}{1-\cos(2\pi l)}\right] \\ &= \frac{1}{4N}\left[2N + 1 - \cos(2N\pi l) + \frac{\cos(\pi l)\sin(2N\pi l)}{\sin(\pi l)}\right] \\ &= \frac{1}{4N}\left[2N + 1 + \frac{\sin[(2N-1)\pi l]}{\sin(\pi l)}\right], \end{aligned}$$

where the first line is derived by comparing the real parts in a summation of exponentials.

3. Casimir operator

The Casimir operator for the algebra is

$$C = S_- S_+ + h(S_z),$$

where the second term satisfies a recursive relation [24]:

$$h(S_z) - h(S_z - 1) = 2R_{N,l} S_z.$$

This relation leads to a solution composed of Bernoulli polynomials:

$$\begin{aligned} h(S_z) &= R_{N,l}\,[B_2(-S_z) - B_2] \\ &= R_{N,l}\left(S_z^2 + S_z\right), \end{aligned}$$

where $B_2(-S_z)$ is the second-order Bernoulli polynomial with the operator S_z as variable and B_2 is the second Bernoulli number. The Casimir operator becomes, then,

$$\begin{aligned} C &= S_- S_+ + R_{N,l}\left(S_z^2 + S_z\right) \\ &= \tfrac{1}{2}(S_+ S_- + S_- S_+) + R_{N,l} S_z^2, \end{aligned}$$

which equals to Eq. (10) and represents a deformed total spin operator S^2.

APPENDIX B: DERIVING THE OPERATION RULES

Assume the eigenstate of the z-spin momentum operator S_z to be $|r,m\rangle$, that is, $r(r+1)$ denotes the total spin number and m the magnetic moment, for which Eqs. (12) and (13) are satisfied. Furthermore, assume $\alpha_m^{(r)}$ to be the coefficients when the ladder operators are applied to the state vectors as in Eqs. (14) and (15), which is indexed by r and m.

By applying the vector $|r,m\rangle$ to the commutation relation Eq. (8), we find

$$\begin{aligned} \langle r,m|[S_+, S_-]|r,m\rangle &= \langle r,m|S_+S_- - S_-S_+|r,m\rangle \\ &= \left(\alpha_{m-1}^{(r)}\right)^2 - \left(\alpha_m^{(r)}\right)^2 \\ &= \langle r,m|2R_{N,l}S_z|r,m\rangle \\ &= 2R_{N,l}m. \end{aligned}$$

Selecting the second and the fourth line, we arrive at a difference equation of m:

$$\left(\alpha_m^{(r)}\right)^2 - \left(\alpha_{m-1}^{(r)}\right)^2 = -2mR_{N,l}.$$

To solve the equation, we list out the iterations until the last entry where $\alpha^{(r)}_{-r-1}=0$ since $-r$ is the minimum value m can take as the magnetic moment:

$$\begin{aligned}\left(\alpha^{(r)}_{m}\right)^2-\left(\alpha^{(r)}_{m-1}\right)^2&=-2R_{N,l}m,\\ \left(\alpha^{(r)}_{m-1}\right)^2-\left(\alpha^{(r)}_{m-2}\right)^2&=-2R_{N,l}(m-1)\\ &\vdots\ \vdots\ \vdots\\ \left(\alpha^{(r)}_{-r}\right)^2-\left(\alpha^{(r)}_{-r-1}\right)^2&=-2R_{N,l}(-r).\end{aligned}$$

Summing up all the iterations above, we have

$$\begin{aligned}\left(\alpha^{(r)}_{m}\right)^2&=-2R_{N,l}\sum_{j=0}^{m+r}(m-j)\\ &=-R_{N,l}(m-r)(m+r+1),\end{aligned}\tag{B1}$$

which gives Eq. (16). We can verify this result by summing up instead of summing down, that is, with the condition $\alpha^{(r)}_{r}=0$ and the iterations,

$$\begin{aligned}\left(\alpha^{(r)}_{m}\right)^2-\left(\alpha^{(r)}_{m+1}\right)^2&=2R_{N,l}(m+1),\\ \left(\alpha^{(r)}_{m+1}\right)^2-\left(\alpha^{(r)}_{m+2}\right)^2&=2R_{N,l}(m+2)\\ &\vdots\ \vdots\ \vdots\\ \left(\alpha^{(r)}_{r-1}\right)^2-\left(\alpha^{(r)}_{r}\right)^2&=2R_{N,l}r,\end{aligned}$$

we have, after adding them up,

$$\begin{aligned}\left(\alpha^{(r)}_{m}\right)^2&=2R_{N,l}\sum_{j=0}^{r-m}(m+j)\\ &=R_{N,l}(r-m+1)(m+r),\end{aligned}$$

which is the same as Eq. (B1).

APPENDIX C: DERIVING THE EXCITATION SPECTRUM OF THE SUPERCONDUCTING QUBIT CHAIN

1. State vector compositions for a general N-qubit superconducting qubit chain

The form into which the system Hamiltonian is split as in Eqs. (17) and (18) ensures that $[H_0,H_1]=0$. The commutation of these two parts implies that we can find simultaneous eigenvectors for H_0 and H_1.

First, for an eigenvector $|n;r,m\rangle$ (or written as $|u,r\rangle$) of H_0, we have

$$H_0\,|n;r,m\rangle=H_0\,|u,r\rangle=\omega_q(m+n)=\omega_q u,$$

where $\{u,n,m\}$ assumes meanings as described in Sec. IV. Note that the eigenvalue $\omega_q u$ is degenerate, for different combinations of m and n that add up to the same u. Therefore the eigenstate of H_0 can be written as a superposition,

$$\begin{aligned}|u,r\rangle&=\sum_{n,m}c_n\,|n;r,m\rangle\,\delta(u-n-m)\\ &=\sum_{n}c_n\,|n;r,u-n\rangle\,\Delta,\end{aligned}\tag{C1}$$

where Δ is a range delta function,

$$\Delta=\begin{cases}1, & -r\leqslant u-n\leqslant r\\ 0, & \text{otherwise,}\end{cases}$$

since we have to ensure the state vectors satisfy the addition rules of angular momentum.

Our next step is to find those of Eq. (C1) that are also simultaneous eigenvectors of H_1. With the modified operation rule Eq. (16) and setting $m=u-n$, we can apply H_1 to the expression and, after reshuffling the terms in the summation such that vectors with the same total excitation number are grouped together, we find

$$\begin{aligned}H_1|u,r\rangle=\sum_n\Big\{&c_n\tilde{\omega}_0 n+c_{n+1}\eta\sqrt{(n+1)}\alpha^{(r)}_{u-n-1}\\ &+c_{n-1}\eta\sqrt{n}\alpha^{(r)}_{u-n}\Big\}|n;r,u-n\rangle\Delta.\end{aligned}\tag{C2}$$

Since ν is the eigenvalue of H_1, we have

$$H_1\,|u,r\rangle=v\,|u,r\rangle=\sum_n c_n v\,|n;r,u-n\rangle\,\Delta.\tag{C3}$$

Then comparing Eq. (C2) with Eq. (C3), we deduce a difference equation,

$$c_{n+1}\eta\sqrt{(n+1)}\alpha^{(r)}_{u-(n+1)}-c_n\tilde{v}_n+c_{n-1}\eta\sqrt{n}\alpha^{(r)}_{u-n}=0,$$

where $\tilde{v}_n=(v-\tilde{\omega}_0 n)/\eta$ and the initial conditions are

$$\begin{aligned}c_{-1}&=0,\\ c_{u+r+1}&=0.\end{aligned}$$

In addition, from the definition of the Δ function, $n\leqslant u+r$.

Now write

$$c_n=\frac{C_n}{\sqrt{n!}\prod_{j=1}^{n}\alpha^{(r)}_{u-j}},\tag{C4}$$

and we have a simplified difference equation,

$$C_{n+1}-C_n\tilde{v}_n+C_{n-1}n\left(\alpha^{(r)}_{u-n}\right)^2=0.$$

To find the solution, we multiply each equation starting with C_j by $\prod_{k=j}^{n}\tilde{v}_n$:

$$\begin{aligned}C_n\tilde{v}_n-C_{n-1}\tilde{v}_n\tilde{v}_{n-1}+(n-1)\tilde{v}_nC_{n-2}\left[\alpha^{(r)}_{u-(n-1)}\right]^2&=0,\\ &\vdots\ \vdots\ \vdots\\ C_2\prod_{j=2}^{n-1}\tilde{v}_j-C_1\prod_{j=1}^{n-1}\tilde{v}_j+C_0\left[\alpha^{(r)}_{u-1}\right]^2\prod_{j=2}^{n-1}\tilde{v}_j&=0,\\ C_1\prod_{j=1}^{n-1}\tilde{v}_j-C_0\prod_{j=0}^{n-1}\tilde{v}_j&=0.\end{aligned}$$

Then with the terminating conditions $C_1=C_0\tilde{v}_0$ and $C_0=1$, we can sum up the equations to eliminate the middle terms and obtain

$$C_n-Q_{0,n-1}+\sum_{j=0}^{n-2}(j+1)C_j\alpha^2_{u-(j+1)}Q_{j+2,n-1}=0,$$

where we use a shorthand notation,

$$Q_{0,n-1} = \prod_{j=0}^{n-1} \tilde{v}_j.$$

To find the analytical expression for C_n, we recursively expand the factor C_j:

$$\begin{aligned} C_n &= Q_{0,n-1} - \sum_{j=0}^{n-2} (j+1) C_j \alpha^2_{u-(j+1)} Q_{j+2,n-1} \\ &= Q_{0,n-1} - \sum_{j=0}^{n-2} Q_{0,j-1} Q_{j+2,n-1} (j+1) \alpha^2_{u-(j+1)} \\ &\quad + \sum_{j=0}^{n-2} \sum_{k=0}^{j-2} Q_{j+2,n-1} Q_{0,k-1} Q_{k+2,j-1} \\ &\quad \times \left[(j+1)\alpha^2_{u-(j+1)}\right]\left[(k+1)\alpha^2_{u-(k+1)}\right] - \cdots \end{aligned}$$

By observing that $Q_{0,j-1} Q_{j+2,n-1} = Q_{0,n-1}/\tilde{v}_j \tilde{v}_{j+1}$ and so on for each pair of Q's in the terms of each recursive expansion, we can recursively factorize out $Q_{0,n-1}$ and arrive at

$$\begin{aligned} C_n = Q_{0,n-1} \sum_{p=0}^{\lfloor n/2 \rfloor} (-1)^p \sum_{\langle j_1 \cdots j_k \cdots j_{\lfloor n/2 \rfloor} \rangle} \cdots \sum, \\ \prod_{k=1}^{p} \frac{(j_k+1)}{\tilde{v}_{j_k} \tilde{v}_{j_k+1}} \left[\alpha^{(r)}_{u-(j_k+1)}\right]^2, \end{aligned}$$

where $\langle j_1 \ldots j_k \ldots j_{\lfloor n/2 \rfloor} \rangle$ is the index set described in Sec. IV. Finally, substituting the above expression back to the transformation Eq. (C4), we can obtain the coefficients of the excitation eigenvector as in Eq. (21).

2. One-excitation spectrum for a four-qubit superconducting qubit chain

The state vector for the one-excitation four-qubit SQC ($u = 1$, $r = 2$, and $m \in \{-2, -1, 0, 1\}$) can be written as

$$|u,r\rangle = c_0|0;2,1\rangle + c_1|1;2,0\rangle + c_2|2;2,-1\rangle + c_3|3;2,-2\rangle.$$

If we assume $c_0 = 1$ as a common factor, the rest of the three coefficients can be written as

$$\begin{aligned} c_1 &= R^{-1/2} \mathscr{C}_{1,0}, \\ c_2 &= R^{-1} \mathscr{C}_{2,0} - \mathscr{C}_{2,1}, \\ c_3 &= R^{-3/2} \mathscr{C}_{3,0} - R^{-1/2} \mathscr{C}_{3,1}. \end{aligned}$$

After plugging in the expression according to Eq. (22), we obtain the expressions shown in Table I.

To find v, and hence the excitation energy, consider the difference equations:

$$\begin{aligned} C_4 - C_3 \tilde{v}_3 + 3C_2 \left(\alpha^{(2)}_{-2}\right)^2 = 0, \\ C_3 - C_2 \tilde{v}_2 + 2C_1 \left(\alpha^{(2)}_{-1}\right)^2 = 0, \\ C_2 - C_1 \tilde{v}_1 + C_0 \left(\alpha^{(2)}_{0}\right)^2 = 0. \end{aligned}$$

Since $C_4 = 0$ and $C_1 = \tilde{v}_0 C_0$, we derive from the last equation:

$$C_2 = C_0 \left[\tilde{v}_0 \tilde{v}_1 - \left(\alpha^{(2)}_0\right)^2\right],$$

and from the first equation,

$$C_3 = 3C_0 \left[\tilde{v}_0 \tilde{v}_1 + \left(\alpha^{(2)}_0\right)^2\right] \frac{\left(\alpha^{(2)}_{-2}\right)^2}{\tilde{v}_3}.$$

Substitute these expressions into the second equation and with Eq. (16), we have

$$\begin{aligned} 12(\tilde{v}_0 \tilde{v}_1 + 6R_{N,l}) R_{N,l} - (\tilde{v}_0 \tilde{v}_1 - 6R_{N,l}) \tilde{v}_2 \tilde{v}_3 \\ + 12 R_{N,l} \tilde{v}_0 \tilde{v}_3 = 0. \end{aligned}$$

Expanding the $\tilde{v}$, we arrive at a fourth-order polynomial equation:

$$\begin{aligned} v^4 - 6\tilde{\omega}_0 v^3 + \left[11\tilde{\omega}_0^2 - 30 R_{N,l}\eta^2\right] v^2 - 6\left[\tilde{\omega}_0^3 - 13\tilde{\omega}_0 R_{N,l}\eta^2\right] v \\ - 36 R_{N,l}\eta^2 \left[\tilde{\omega}_0^2 + 2R_{N,l}\eta^2\right] = 0. \end{aligned}$$

If we consider the case with $\tilde{\omega}_0 = 0$ (the conventional TC-model case), we have

$$v^4 - 30 R_{N,l}\eta^2 v^2 - 72 R_{N,l}^2 \eta^4 = 0,$$

and the roots are

$$v = \pm\sqrt{(15 + 3\sqrt{33}) R_{N,l}}\,\eta.$$

On the other hand, if we consider a weak coupling case $\tilde{\omega}_0 \gg \eta$, then the equation becomes

$$v^4 - 6\tilde{\omega}_0 v^3 + 11\tilde{\omega}_0^2 v^2 - 6\tilde{\omega}_0^3 v - 36 R_{N,l}\eta^2 \tilde{\omega}_0^2 = 0,$$

and the solutions are

$$v = \frac{3}{2}\tilde{\omega}_0 \pm \frac{1}{2}\sqrt{5\tilde{\omega}_0^2 \pm 4\tilde{\omega}_0 \sqrt{\tilde{\omega}_0^2 + 36 R_{N,l}\eta^2}}.$$

Hence, the excitation energy can be written as in Eq. (23).

Now the coefficient c_1 for the highest eigenenergy state is, since usually $\tilde{\omega}_0 < 0$,

$$c_1 = \frac{v}{\sqrt{6R_{N,l}}\,\eta} = \frac{3}{2}\Omega + \frac{1}{2}\sqrt{5\Omega^2 - 4\Omega\sqrt{\Omega^2 + 6}},$$

where $\Omega = \tilde{\omega}_0/(\eta\sqrt{6R_{N,l}})$. Since $R_{N,l} \leqslant 1$,

$$|\Omega| \geqslant \left|\frac{\tilde{\omega}_0}{\sqrt{6}\eta}\right|,$$

which means that the deformation leads to a larger coefficient c_1 than that of the undeformed case. For c_2, we have

$$c_2 = \frac{1}{\sqrt{2}}\left(c_1^2 - \Omega c_1 + 1\right) > \frac{1}{\sqrt{2}}(c_1 + 1)^2,$$

since $\tilde{\omega}_0 \gg \eta$ and so $|\Omega| \gg 2$. This means that c_2 increases by a greater proportion than c_1 due to the deformation. Similarly, c_3 increases by an even larger factor. The change in the coefficients shows that a larger deformation favors the states with a larger number of photons and a more ordered spin chain.

[1] J. Q. You and F. Nori, Phys. Rev. B **68**, 064509 (2003); J. Q. You, J. S. Tsai, and F. Nori, *ibid*. **68**, 024510 (2003).
[2] A. Blais, R.-S. Huang, A. Wallraff, S. M. Girvin, and R. J. Schoelkopf, Phys. Rev. A **69**, 062320 (2004).
[3] J. Hauss, A. Fedorov, C. Hutter, A. Shnirman, and G. Schön, Phys. Rev. Lett. **100**, 037003 (2008).
[4] H. Ian, Y.-X. Liu, and F. Nori, Phys. Rev. A **81**, 063823 (2010).
[5] S. N. Shevchenko, S. Ashhab, and F. Nori, Phys. Rep. **492**, 1 (2010).
[6] J. Q. You and F. Nori, Nature (London) **474**, 589 (2011).
[7] C. M. Wilson, G. Johansson, A. Pourkabirian, M. Simoen, J. R. Johansson, T. Duty, F. Nori, and P. Delsing, Nature (London) **479**, 376 (2011).
[8] J. Q. You and F. Nori, Phys. Today **58**, 42 (2005).
[9] Y.-X. Liu, C. P. Sun, and F. Nori, Phys. Rev. A **74**, 052321 (2006).
[10] F. Helmer, M. Mariantoni, A. G. Fowler, J. von Delft, E. Solano, and F. Marquardt, Europhys. Lett. **85**, 50007 (2009).
[11] I. Buluta, S. Ashhab, and F. Nori, Rep. Prog. Phys. **74**, 104401 (2011).
[12] A. L. Rakhmanov, A. M. Zagoskin, S. Savel'ev, and F. Nori, Phys. Rev. B **77**, 144507 (2008).
[13] S. Savel'ev, V. A. Yampol'skii, A. L. Rakhmanov, and F. Nori, Rep. Prog. Phys. **73**, 026501 (2010).
[14] J. M. Fink, R. Bianchetti, M. Baur, M. Göppl, L. Steffen, S. Filipp, P. J. Leek, A. Blais, and A. Wallraff, Phys. Rev. Lett. **103**, 083601 (2009).
[15] Y.-D. Wang, F. Xue, Z. Song, and C.-P. Sun, Phys. Rev. B **76**, 174519 (2007).
[16] N. Lambert, Y.-N. Chen, R. Johannsson, and F. Nori, Phys. Rev. B **80**, 165308 (2009).
[17] P. Nataf and C. Ciuti, Phys. Rev. Lett. **104**, 023601 (2010).
[18] L. Tian, Phys. Rev. Lett. **105**, 167001 (2010).
[19] I. Buluta and F. Nori, Science **326**, 108 (2009).
[20] I. Diniz, S. Portolan, R. Ferreira, J. M. Gérard, P. Bertet, and A. Auffèves, Phys. Rev. A **84**, 063810 (2011).
[21] R. H. Dicke, Phys. Rev. **93**, 99 (1954).
[22] A. P. Polychronakos, Mod. Phys. Lett. A **5**, 2325 (1990).
[23] M. Roček, Phys. Lett. B **255**, 554 (1991).
[24] C. Delbecq and C. Quesne, J. Phys. A **26**, L127 (1993).
[25] D. Bonatsos, C. Daskaloyannis, and P. Kolokotronis, J. Phys. A **26**, L871 (1993).
[26] M. Tavis and F. W. Cummings, Phys. Rev. **170**, 379 (1968).
[27] S. Swain, J. Phys. A **5**, L3 (1972); C. E. López, H. Christ, J. C. Retamal, and E. Solano, Phys. Rev. A **75**, 033818 (2007).
[28] M. Reed and B. Simon, *Methods of Modern Mathematical Physics* (Academic Press, San Diego, 1980).
[29] W. Y. Liang, Phys. Educ. **5**, 226 (1970).
[30] J. Knoester, Phys. Rev. Lett. **68**, 654 (1992).
[31] H. Deng, H. Haug, and Y. Yamamoto, Rev. Mod. Phys. **82**, 1489 (2010).
[32] J. C. Slater and W. Shockley, Phys. Rev. **50**, 705 (1936).
[33] S. Blumstengel, S. Sadofev, C. Xu, J. Puls, and F. Henneberger, Phys. Rev. Lett. **97**, 237401 (2006).